Two-phase microfluidics in electrowetting displays and its effect on optical performance

Tao He,[1] Mingliang Jin,[1,a)] Jan C. T. Eijkel,[2] Guofu Zhou,[1,3] and Lingling Shui[1,a)]
[1]*Institute of Electronic Paper Displays, South China Academy of Advanced Optoelectronics, South China Normal University, Guangzhou 510006, Guangdong, China*
[2]*BIOS/Lab-on-a-Chip group, MESA+ Institute for Nanotechnology, University of Twente, Enschede, The Netherlands*
[3]*Academy of Shenzhen Guohua Optoelectronics, Shenzhen 518110, Guangdong, China*

(Received 27 October 2015; accepted 29 January 2016; published online 11 February 2016)

Driving microfluidic flow in micropixels by electrowetting to realize light switches and displays is of both practical and fundamental significance. The electro-optical performance related to microfluidic behavior needs to be clarified to optimize device functions. In this article, the microfluidic performance in electrowetting display devices was categorized according to the oil-water interface shape and response. The oil film movement was divided into vertically "thinning" and transversally "opening," for which the "thinning" process was found the key factor determining the pixel switching speed rather than the "opening" process. Therefore, the breakup point and the oil film thickness were critical, which could be controlled by surface wettability and oil volume. We have also realized a new oil filling method with controllable dosing volume assisted by the microfluidic creation of microdroplets. This study could help quantitatively understand electrowetting display performance in both its theoretical and practical aspects. © *2016 AIP Publishing LLC*.
[http://dx.doi.org/10.1063/1.4941843]

I. INTRODUCTION

The growing interest in electrowetting on dielectric (EWOD) has led to a wide range of scientific and technological investigations motivated by its applicability in digital microfluidics,[1–3] lab-on-a-chip systems,[2–4] and droplet-based optofluidics.[5–9] Microlenses, electrowetting displays, and optical switches are the typical examples of electrowetting optofluidic systems.[10] Electrowetting could vary and control the wettability of a solid surface by an externally applied voltage.[9,11–14] It is generally agreed that electrowetting is one of the most flexible tools which could achieve reversibility,[15,16] reproducibility,[17] and mobility[3,18] in microdevices.

The fundamental understanding of the electrowetting fluidic dynamics[19–23] and non-equilibrium molecular dynamics (NEMD) code[4,24] have been developed. Most studies have been done by actuating millimeter-sized aqueous sessile droplets on flat solid surfaces by direct current (DC) electrowetting.[17,25–30] In a range of voltages, the contact angle changes with the applied voltage corresponding to the Young-Lippmann equation

$$\cos\theta(V) = \cos\theta(0) + \frac{1}{2\gamma_{gl}} CV^2, \tag{1}$$

where $\theta(0)$ and $\theta(V)$ are the contact angles of a water droplet on a hydrophobic surface without (0) and with an applied voltage (V); γ_{gl} is the interfacial tension between liquid and gas; C is the capacitance per unit area which in our case is the constant capacity across the insulator layer,

[a)]Author to whom correspondence should be addressed. Electronic addresses: jinml@scnu.edu.cn and shuill@m.scnu.edu.cn. Tel.: 86-(20)-3931 4813. Fax: 86-(20)-3931 4813.

described by $C = \varepsilon_0\varepsilon_r/d$ with ε_0 and ε_r being the dielectric constant of vacuum and the relative dielectric constant of the insulator layer, and d, the thickness of the insulator layer.[31] The advantages of electrowetting include reversibility, contactless control, low voltage driving, and materials biocompatibility for which this technology has been used to drive droplets,[1,17,21,22,28,30,32–34] display information,[35–39] microlenses,[9] prisms,[40] and colloidal particle assembly.[41]

The application of electrowetting for displays was proposed by Beni and Hackwood in 1980s,[42,43] however, the impressive video-speed display devices were only realized by Hayes and Feenstra in 2003.[35] In the last decade, this technology has been widely studied.[44–50] Color switching of the electrowetting display is realized by showing the color of a dyed oil film or the underneath substrate by applying a voltage in the range of 0-V voltages. Currently, the companies of Amazon, Gamma Dynamics, ADL, ITRI, Etulipa, and Guohua Optoelectronic Co. Ltd. are working on the industrialization of the electrowetting display technology.[36]

The detailed device structure and performance are demonstrated in Fig. 1. The standard configuration of an electrowetting display device consists of the bottom substrate with electrodes and hydrophobic insulator layer, hydrophilic grids (pixel walls), colored oil, conductive liquid, and the top electrodes on the cover substrate (Fig. 1). The response of the electrowetting effect highly depends on the properties of the materials of the different functional layers. Particularly, the properties of the hydrophobic insulating layer are known to play an important role in electrowetting devices.[18] To obtain a wide contact angle change with low voltage, a high initial contact angle of the conductive liquid is preferred. Multilayer materials have also been studied to achieve both insulating and hydrophobic functions, for instance, the inorganic insulating materials like SiO_2, Si_3N_4, SiOC, or ONO (oxide-nitride-oxide) combined with a hydrophobic coating layer.[14,32] This offers a larger contact angle change at the same applied voltage due to their higher value of the dielectric constant. The amorphous fluoropolymers with low surface energy were typically used in the electrowetting display as a hydrophobic insulator, for example, AF1600,[15,51] FluoroPel 1601 V,[2,52] Cytop CTL-809M,[53] and fluorinated polyimide.[54]

In the electrowetting display devices, except for the hydrophobic insulator and the micropixel wall, the dyed oil and conductive liquid materials are also critical for the display performance.[46,55–58] In this article, we chose AF 1600 as the hydrophobic insulator, SU-8 3005 as the micropixel wall material, and Keyston Blue dissolved in dodecane as the dyed oil for reason of its stability and widely investigated properties. A 0.1 wt. % NaCl aqueous solution was used as the conductive liquid phase. As seen from Fig. 1, the conductive liquid filled the gap between the oil and the top plate (electrode), driving the dye oil and moving it when actuated by electrowetting.

To fill both the non-conductive dyed oil and conductive aqueous phase into the display device homogeneously without bubbles, a self-assembly method was typically applied.[38] The volume of the oil inside the micropixel was sensitive to both materials properties and filling process parameters. In the published literature, we found that the resulting oil distribution in the micropixel was different. The oil-water interface was found concave (negative) with respect to the oil phase in Refs. 56 and 59 and convex (positive) with respect to the oil phase in Refs. 35, 55, 57, and 60–62. Properties like the interaction between liquid and solid phases (surface tension,

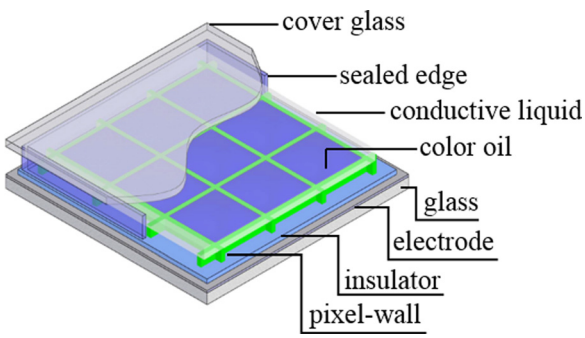

FIG. 1. Schematic drawing of the electrowetting display device.

contact angle), the filling speed, and the oil film between air and oil during filling could all affect the filled volume and homogeneity of the dosed oil in the pixels. According to different oil distribution models, the typical oil film breakup and redistribution inside the confined micropixel are also different, which in the end affects the response time (display speed) and the white area fraction (opening fraction) of the micropixels.

In this article, we investigate the details of the oil film distribution modes in the micropixels of electrowetting display devices and categorize them into four modes according to the oil volume. We have carefully studied the fluidic flow in the micropixels and propose a mechanism of the oil film breakup and oil movement in the micropixel. For the first time, we find that the oil film thinning process is the main factor determining the switching speed which is one of the critical parameters when evaluating a display device. To control the volume of the dosed oil in each micropixel, we propose a new dosing method by combining the self-assembly filling with pre-generated oil droplets using a microfluidic device. The oil droplet volume could be precisely controlled by the pre-prepared oil droplet in a microfluidic device. With the success of this approach, we could control the oil volume in the micropixel on-demand, which helps better control the optical performance of electrowetting devices.

II. EXPERIMENTAL

A. Device fabrication

The indium tin oxide (ITO) coated glass (0.7 mm thick) with square resistance of 100 Ω/□ was used as the electrodes and supporting substrate (Shenzhen Laibao Hi-tech Co. Ltd., China). DuPont Teflon AF 1600 was used as the hydrophobic insulator layer which was spin-coated on the electrode layer with a dry film thickness of about 800 nm.[63] Subsequently, the hydrophobic surface was treated to become hydrophilic using oxygen plasma equipment (ME-6A, Institute of Microelectronics, Chinese Academy of Science, China). The hydrophilic grids were patterned using SU-8 3005 (Microchem Corp, Newton, MA, USA) by photolithography.[63] The obtained film thickness and grid size were measured by a Dektak XT (BRUKER, Germany). The pixels were 150 μm × 150 μm with grid height and width about 6 and 15 μm, respectively. Colored oil and conductive liquid was then filled and sealed with a cover plate to form an electrowetting display device.

B. Blue dye preparation

The blue dye was purchased from Keystone, USA. The dye was first purified before using. The dye solution was subjected filtration process through a silica gel column (300–400 mesh, Haiyang Chem., China). The top of the gel column revealed a thin black-colored layer which was due to impurities. Thin-layer chromatography (TLC) was then used to further separate the undesirable impurities from the dye.[39] After purification, the blue dye was dissolved in n-dodecane (Aladdin, GC, China) and used as the colored oil.

C. Contact angle measurement

The ITO substrates coated with 800 nm AF 1600 and 6 μm SU-8 3005 were placed under ultra-pure water, and then oil droplets were pumped onto the surface of AF 1600 and SU-8 3005 using micro-injector, surrounded by water. The contact angle of oil droplets on AF 1600 and SU-8 3005 surrounded by water was measured by a contact angle meter OCA 15 Pro (Dataphysics, Germany).

D. Microdroplets creation

Monodisperse microdroplets of dyed oil were created using a flow-focusing glass microfluidic chip purchased from Micronit Microfluidics, the Netherlands. A syringe pump (KD Scientific, Hong Kong, China) was used for fluidic pumping. A high speed camera (Phantom MIRO M110, Vision Research, USA) integrated with a microscope (CKX41, Olympus, Japan)

was used for observing the fluidic behavior in the microfluidic chip. Colored oil droplets with a size of $\sim 50\,\mu$m were produced in the flow-focusing glass chip with outer and inner phase flow rates of 0.1 and 0.01 ml/h, respectively. The microdroplets were then flowed out through a micro-tube to a glass bottle filled with de-ionized (DI) water and ready for the self-assembly filling process.

E. Electrowetting display device test

To quickly test the electrowetting display device, a drop of blue oil (1–2 μl) was purged on the pixelated plate, and then covered with aqueous solution. The electrical circuit was realized with a metal wire electrode inserted into the aqueous solution, and the other electrode was directly connected to the conductive ITO layer underneath the insulator layer. Both electrodes were connected to an impedance analyzer (6500B, WAYNE KERR, Britain) which was used to perform the electrical driving and measurements. The oil motion was then visualized and recorded by the high speed camera/microscope setup.

III. RESULTS AND DISCUSSION

The electrowetting display functions by switching the micropixels to show the oil film color or the underneath substrate color when the oil film fully fills the pixel or is contracted to the corners, respectively. With an opaque bottom substrate, the incident visible light is reflected depending on the dye and substrate materials. The response time is determined by the oil motion, and the optical property is dependent on the electrical force and the pixel structure.

A. Switching modes in micropixels

Seemann *et al.*[11] have studied the wetting morphologies of liquid at microstructured surfaces, demonstrating various interface morphologies controlled by the liquid volume, surface wettability, and microstructure geometry. In square microwells, the liquid distributed as a continuous film or a concave interface (negative to air) without breaking if the contact angle was $<45°$; however, the liquid distributed as small droplets sticking to the corners or a convex interface (positive to air) when the contact angle was $>45°$.

In our experiments, when the dyed oil solution touches the fluoropolymer surface, it will be attracted to and spread over the micropixel surface due to the hydrophobic interaction between the hydrophobic AF 1600 and dodecane solution. In electrowetting display devices, the oil typically stays inside the pixel surrounded by the pixel walls with the bottom contacted to the fluoropolymer surface and the top exposed to the conductive water phase. The oil film morphology therefore varies with the oil volume and the surface wettability of the pixel. To demonstrate the different morphological modes of the oil distribution in micropixels, we performed the experiments on a pixelated plate and successfully obtained four types of typical modes, as shown in Fig. 2(a). This figure shows that the interface morphology changed with the quantity of added oil. Modes 1 and 4 were obviously under-filled and over-filled statuses with incomplete oil film and coalesced oil droplets, respectively. These two modes were not applicable for electrowetting display. In modes 2 and 3, the oil spontaneously filled the micropixels forming complete oil films but with different oil-water interface curvatures, facing the oil and water phases, respectively.

When -40 V voltage was applied on the bottom electrodes, all oil droplets started to move transversally after a short period of time and reached the final states as shown in Fig. 2(b). In mode 1 pixels, the oil film coverage was not complete with an opening in the center of the film where the film started to spread immediately with the applied voltage. The oil then became attached to the corners of the micropixels and difficult to completely recover after the electrical field was released. For the big merged blue drop in mode 4, when the voltage was applied, it started to contract whereby the edges digitally moved towards the center. This agreed with the Wenzel mode of structured hydrophobic surface.[13,64,65] The drop spread again after turning off the electrical field.

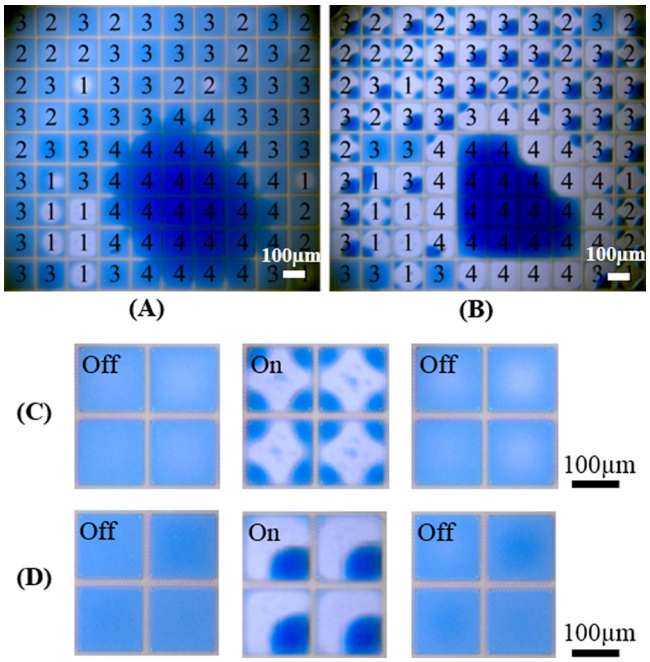

FIG. 2. Microscopic images of oil-water two-phase fluidic distribution in micropixels with different amount of oil without (a) and with an applied voltage of −40 V (b). The four modes of the pixels are categorized into (1) under-filled oil with incomplete oil film, (2) suitable amount of oil with a negative interface curvature to oil, (3) suitable amount of oil with a positive interface curvature to oil, and (4) over-filled oil forming a merged big oil drop. (c) and (d) The off-on-off states for modes 2 and 3, respectively. The oil and water are blue oil and 0.1 M NaCl aqueous solution, respectively.

Because of the incomplete film and merged oil drop, modes 1 and 4 were not further considered hereafter. Both modes 2 and 3 pixels could reversibly open and close by the electrowetting effect (see Figs. 2(c) and 2(d)) which could satisfy the requirement for electrowetting displays; however, they demonstrated different microfluidic behavior. Therefore, modes 2 and 3 were investigated in detail as reported in the following.

In mode 2, the oil-water interface was concave from top view (negative curvature to oil phase). When a voltage was applied, the oil film was broken from the center of the micropixel where the oil film was thinner, and then each part of the film moved towards the four corners and formed smaller droplets. When the electrical field was released, the four oil droplets flowed back to the pixel center and reunited to form a complete oil film (Fig. 2(c)). Analyzing mode 3, we found that a convex interface (positive to the oil phase) existed between oil and water phase. The oil film was broken from the edge and pushed aside to one of the corners, forming a large oil droplet standing adjacent to the pixel walls which spread back re-forming an oil film when the driving field was turned off (Fig. 2(d)).

To obtain more information, we analyzed the grayscale pattern of the image of a single micropixel, as shown in Figs. 3(a) and 3(c) for the original (closed) and final (open) states with an applied voltage of −40 V of mode 2 pixel, and Figs. 3(b) and 3(d) for the original (closed) and final (open) states with an applied voltage of −40 V of mode 3 pixel. The intensity through the pixel diagonal showed that the oil-water interface curvature was not simply like shown in the reference[11] since in our case the pixel was made of two different materials: AF 1600 and SU-8 3005. The interface curvature was thus determined by both surfaces of the hydrophilic grids and the hydrophobic Teflon. The contact angle of the oil droplet surrounded by water on SU-8 3005 was 80.5° (>45°) and on AF 1600 was much smaller than 45° (a more precise value was difficult to measure using current instrument because the oil phase spreads widely on AF 1600 surface according to the hydrophobic interaction). In our experimental device, the pixel height and length are 6 μm and 150 μm, respectively, giving an aspect ratio (height/length) of the micropixel of 0.04. The oil film profile in micropixels experienced the under-filled

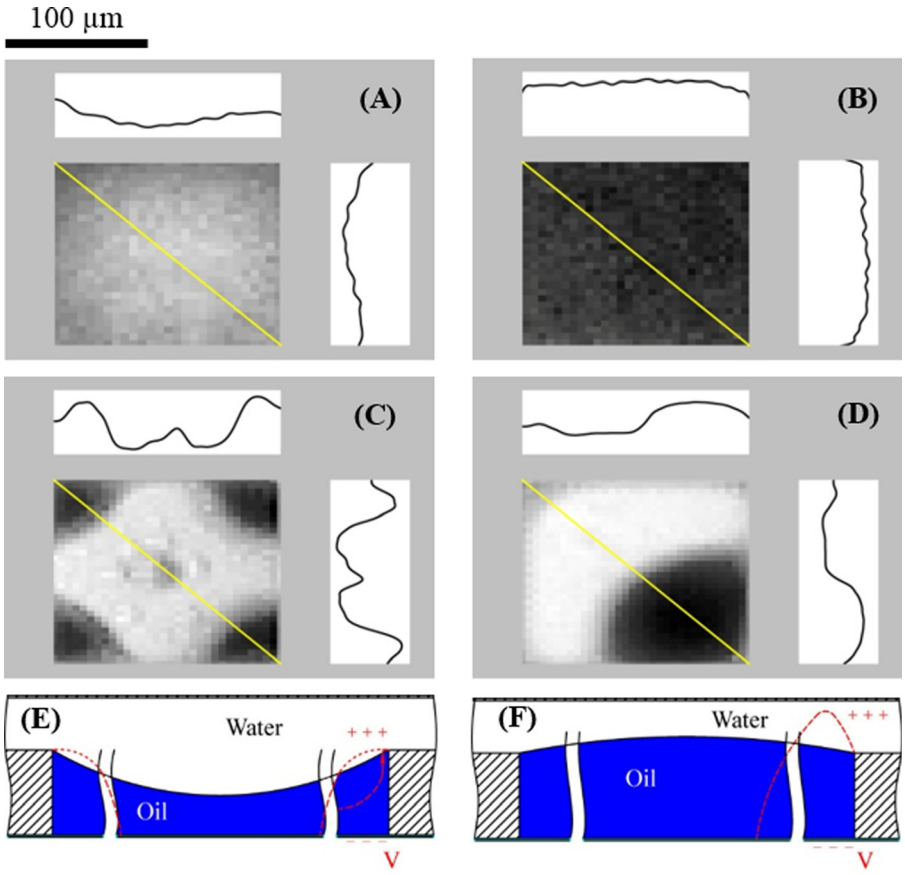

FIG. 3. Oil-water microfluidic performance in modes 2 and 3 of the electrowetting display pixels. (a) and (b) The microscopic images of the original status of modes 2 and 3. (c) and (d) The microscopic images of the final status of modes 2 and 3 with an applied voltage of −40 V. (e) and (f) The schematic diagrams of the oil-aqueous solution interface movement with applying a voltage (red line) in modes 2 and 3. The profile lines attached in A, B, C, and D are the grayscale profiles of the oil-water interface along the pixel diagonal (yellow line) extracted from the microscopic images.

(mode 1), concaved film (mode 2), convex film (mode 3), and over-filled (mode 4) with addition of the oil volume, which is agreed with the proposed mechanism.[11] The extracted X-axis and Y-axis interface profiles are shown on the top and right of the images of Figs. 3(a)–3(d). The initial status showed that the pinned film in the pixel was determined by the volume of the oil and the contact angle of pixel material. When a voltage was applied, the hydrophobic AF 1600 surface became hydrophilic, and water started to be attracted to it. The oil film then broke either from the pixel center or from the edge where the oil film was the thinnest. After film breaking, the oil was pushed forward by the wetting water to the pixel wall and corners to let more water come into contact with the hydrophilic surface. In the end, oil accumulated at the corners forming pinned droplets and exposing the underneath substrate showing its color. The schematic drawings of the interface moving are shown in Figs. 3(e) and 3(f). In mode 2, the small droplets left in the center was formed by the film breakup caused by the instability of thin oil film.[66,67] In mode 3, such small satellite droplets were seldom found because the film was thicker.

B. Electro-optical performance

The purpose of the electrowetting display is to obtain optical variation via microfluidic movement driven by an electrical field. This is dependent on the response of the water phase to the applied voltage, which then drives the oil film to move resulting in an optical switch. Therefore, the microfluidic dynamics is very important in this device. We recorded the detailed

process of the film breaking and moving using a high speed camera. By analyzing thousands of microscopic images of each process with millisecond time resolution, we obtained both the optical properties and response time in each stage.

The optical performance was evaluated by the white area fraction which was calculated by

$$WA\% = \left(1 - \frac{A_{oil}}{A_{pixel}}\right) \times 100, \tag{2}$$

where A_{oil} and A_{pixel} are the area occupied by oil and the overall pixel area, respectively. The white area fraction changed with time for modes 2 and 3 as shown in Figs. 4(a) and 4(b).

The results demonstrated clearly that the maximum white area fraction of mode 2 was ~45% which was smaller than the value of mode 3 of ~55%. However, the pixel switching speed of mode 2 was higher than that of mode 3. Categorizing the process by inspecting the time dependence of the *WA%* as well as the high-speed recordings, we found that the whole process could be divided into three stages: "thinning," "opening," and "stabilizing" (see the inset of Fig. 4(a)). When a voltage was applied, the film thinning was started without its transversal position changing from the top view. This process was called the "thinning" stage. In the "thinning" stage, the top view image did not show oil film opening (transversal) movement. This process is normally missed if the millisecond movement cannot be caught continuously using a high speed camera.[68] The oil film was "broken" when the film stopped thinning and started opening. In the next stage, the oil film moved towards the corners. This stage was named the "opening" stage, and it was accompanied by an obvious rapid change in the white area fraction. The "opening" stage stopped when most of the oil had reached the walls after which a stable situation was reached which was named the "stabilizing" stage in which the *WA%* only varied slightly. Hydrodynamically, during the "thinning" stage, the water phase travels vertically towards the Teflon to break the oil film; during the "opening" stage, it increasingly wets the Teflon, pushing the oil to move transversally to achieve optical opening of the pixel till the "stabilizing" stage with only small further changes of the oil shape occurring.

Fig. 4 shows the stages categorization and the experimental results. The "thinning" stage of mode 2 was much shorter than mode 3, on average 2.5 ms and 16.5 ms, respectively. The average time for "opening" was 6.5 ms and 11.5 ms for modes 2 and 3, respectively. Therefore, the total switching time was about 9.0 ms and 28.0 ms for modes 2 and 3. It is also obviously seen from the error bars in Fig. 4(b) that the time of the "opening" process was more constant and the time variation between modes 2 and 3 was small. However, the time needed for the "thinning" process varied a lot between modes 2 and 3 in the range from 1.8 ms to 22.5 ms, a difference with a factor of 12.5. The time for "thinning" process could be either shorter (0.1 times) or longer (5.5 times) than the "opening" time. This could be explained as following. The plane pixel size was standard (150 μm × 150 μm), and the maximum *WA%* variation was insignificant

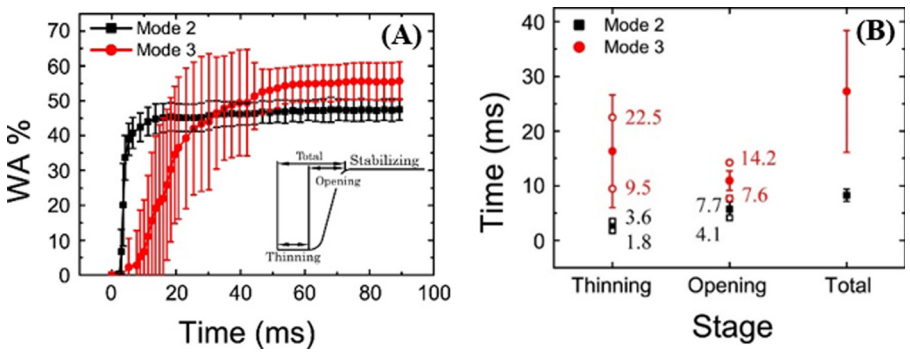

FIG. 4. (a) White area fraction versus time of pixels for modes 2 and 3. Inset is the schematic drawing of the three microfluidic moving stages. (b) Operation time of different oil film moving stages for modes 2 and 3. The error bars show the standard deviation of the values, and the hollow symbols represent the minimum and maximum values of the processes.

as shown in Fig. 4(b), which meant that the transversal moving distance showed no big difference for the same mode. However, the film thickness could be very different depending on the dosed oil volume in each pixel, and therefore, the vertical travelling distance varied a lot. This meant that the "thinning" stage rather than "opening" stage caused big differences in the pixel opening speed. This behavior is different from we originally thought, and it is also different from most published results. The difference can be ascribed to the use of the high-speed camera enabling a high spatial and temporal resolution study of the single pixel switching process in the electrowetting display device, resulting in the optical performance. Based on this result, we found out that the key parameter to achieve higher speed and larger open area fraction in the same electrowetting display device is the filled oil amount. On the other hand, it requires a more precise dosing technology to control the oil film thickness in every pixel equally and satisfy the quantitative investigation.

C. Dosing with controllable volume using microfluidic created oil droplets

As discussed in Sec. III B, the oil film thickness in the pixel is very important for the switching speed. In general, the electrowetting pixel is filled using the self-assembly method,[38] as schematically demonstrated in Fig. 5(a). The dyed oil is poured on the water surface forming a thin film which is filled into the pixels when the water-oil interface moves along the pixelated substrate. This method is sensitive to the oil film properties (thickness, surface tension, viscosity) between the air and water phase, the moving speed of the oil-water interface, and the surface properties of the AF 1600 and SU-8 3005 grids. Therefore, the obtained oil volume in the micropixels is not constant in different experiments. The dosed oil volume furthermore varies with the

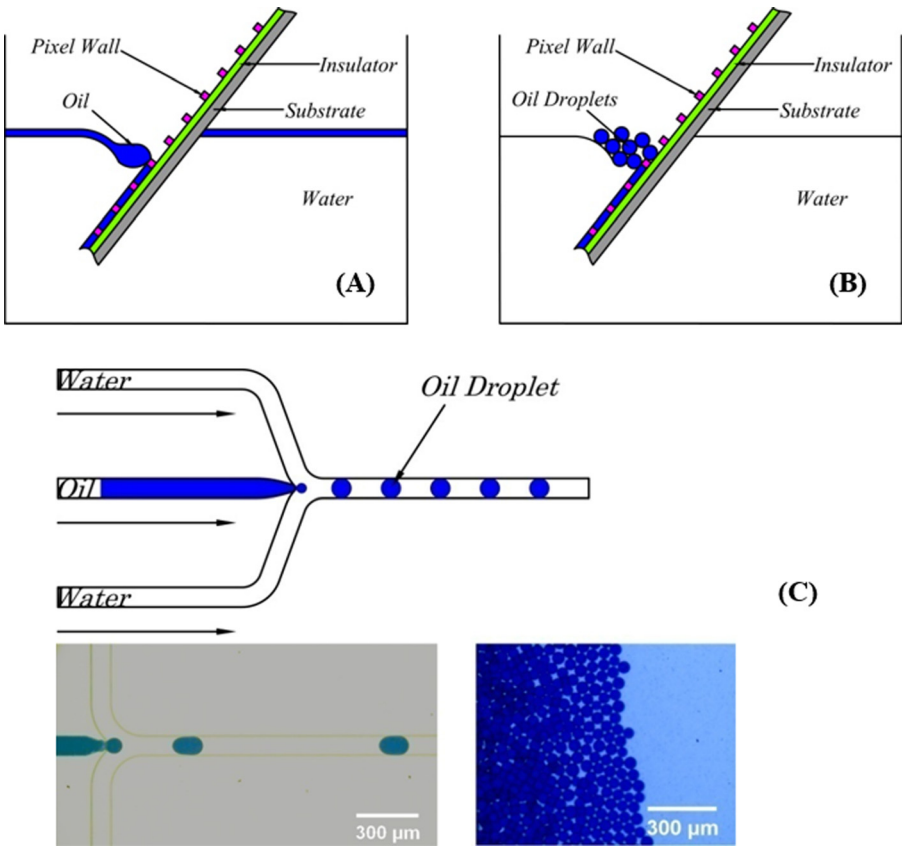

FIG. 5. (a) Schematic of the normal self-assembly oil dosing method. (b) New dosing method of combining self-assembly and microdroplets. (c) Microfluidic droplet generation device: flow focusing microfluidic structure (top), blue oil droplet generation in microfluidic device (bottom left) and generated oil droplets before dosing.

oil type, conductive liquid, the materials and the aspect ratio pixel materials, and the stability and speed of filling process. We see this as the reason why the literature has shown different images of filled pixels.[35,55,57,60,62,69] Here, we propose and have realized a new method of precisely dosing oil into micropixels by combining the self-assembly method with microfluidic droplets with pre-defined volume. The schematic view of the new method is shown in Fig. 5(b) by combining the normal self-assembly dosing method (Fig. 5(a)) and microdroplets (Fig. 5(c)).

We used a glass microfluidic chip with flow-focusing junction to create monodisperse microdroplets with precisely controlled volume. Oil droplets with a diameter of about 50 μm were obtained and then exported out of the device via a microtube into a glass bottle filled with 0.01 wt. % SDS aqueous solution, as shown in Fig. 5(c). The oil droplets on the water

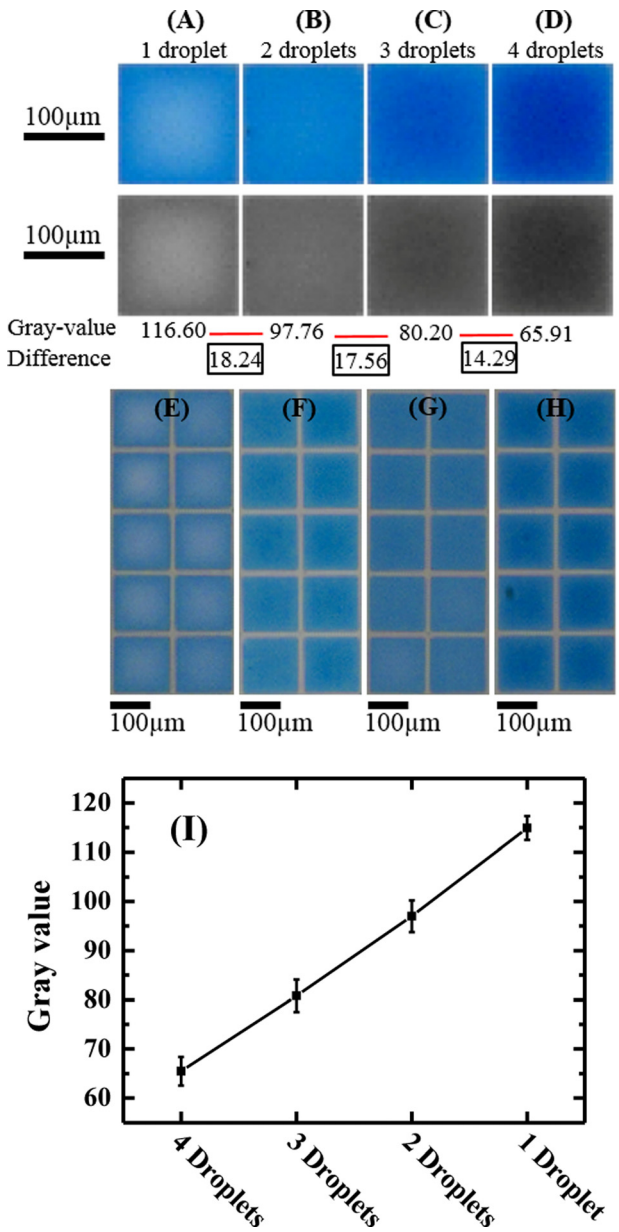

FIG. 6. Digitally dosed micropixels. (a)–(d) Microscopic photos (top) and corresponding black and white images extracted from the top images for pixels filled with one droplet (a), two droplets (b), three droplets (c) and four droplets (d). (e)–(h) Microscopic images of multiple pixels filled with one, two, three, and four droplets, respectively. (i) Average gray scale versus droplets numbers in each pixel with the standard deviation out of 100 pixels.

surface were then introduced into a self-made filling tank for dosing the micropixels by the self-assembly method.

In the normal self-assembly method, the oil film on the water is continuous. The dosing volume is then determined by the factors discussed before. In this new method, since the oil droplets are individual, single droplet dosing could be achieved. By controlling the number of droplets per pixel, we obtained pixels filled with controllable oil volumes, for which the exact film thickness could be calculated. Fig. 6 shows the results of obtained pixels filled with one, two, three, and four droplets ($\sim$50 μm diameter). The droplet and pixel volume were 65.4 pl and 135.0 pl, respectively. Therefore, in Figs. 6(a)–6(d), the exact oil volume in the pixel was 65.4, 130.8, 196.2, and 261.6 pl, which was 0.48, 0.97, 1.45, and 1.94 times the pixel volume, respectively. Therefore, the minimum and maximum film thickness for A, B, C, and D could be calculated later. By analyzing the grayscale of these images, we obtained an average intensity of each pixel of 113.6, 97.8, 80.2, and 65.9, and an intensity difference between two neighboring pixels of 15.8, 17.6, and 14.3, respectively. This confirms that the volume of the oil in the pixels increases digitally with the number of dosed oil droplets. Pixels of Figs. 6(a)–6(d) represent modes 1, 2, 3, and 3, respectively. Figs. 6(e)–6(h) demonstrate ten pixels filled with one, two, three, and four droplets, respectively. Fig. 6(i) shows the average gray scale value and standard dievation obtained from 100 pixels for each point. The number of droplets filled in pixel could be controlled by density of oil droplets on surface, water moving speed and number of filling cycles. By carefully controlling the filling speed, we did not obtain under-filled pixels corresponding to mode 1 or over-filled pixels corresponding to mode 4. The use of separated oil droplets instead of the continuous oil film during self-assembly filling process thus has the substantial additional advantage of avoiding under-filled micropixel (mode 1) and over-filled micropixels (mode 4) which are detrimental for a display device.

This new filling methodology shows controllable oil volume dosing in micropixels. On the one hand, this is very important for further quantitative understanding of the microfluidic behavior in electrowetting devices. On the other hand, it can help improving the electrically driving optical performance via controlling the microfluidic parameters.

IV. CONCLUSION

The electrowetting display is of practical interest to both academic and industrial researchers. Although there has been a lot of work done in this area, the fundamental understanding of the microfluidic behavior related to the opto-electrical performance is still lacking. By carefully investigating micropixels of electrowetting displays, we proposed four pixel filling modes according to the difference in oil film integrity and microfluidic behavior. Modes 2 and 3 represented two typical functional pixels, for which oil-water interface curvatures were negative and positive with respect to the oil phase, whereby the interface distribution was determined by the oil volume and surface wettability. On switching the oil film was found to break from the pixel center or the edge of films based on its initial thickness distribution. Surprisingly, we found that, compared to the pixel "opening" stage (in which the water and oil phase moved horizontally driven by electrowetting), the preceding oil film "thinning" process (in which the water phase moved vertically) played the key role in determining the switching speed of a micropixel. To obtain quantitative oil dosing in the micropixels to optimize the switching speed, we proposed and successfully realized a new filling method which was assisted by precisely controlled oil droplets created by using a microfluidic device. This methodology could not only control the dosing volume but also avoid the failure modes of under-filled (mode 1) or over-filled (mode 4) micropixels. By precisely analyzing the microfluidic behavior in the micropixels assisted by the new controllable volume dosing method, we hope it will be possible to further quantitatively understand the electrowetting performance. Overall, our results can be of great help to optimize the design of electrowetting display and other electrowetting driven devices like microlenses, digital microfluidics, microprisms, microfluidic arrays and so on.

ACKNOWLEDGMENTS

We would like to thank Rob A. Hayes for fruitful discussion, Yingying Dou and Hao Wu for their help in cleanroom, Xiao Zhang, Hongwei Jiang, Xia Chen, Yunfei Zhu, and Xiange Li for their help in measurements. We appreciate the financial support from National Natural Science Foundation of China (Nos. 61574065 and 21303060), program for Changjiang Scholars and Innovative Research Team in University (IRT13064). This work was also supported by Guangdong Natural Science Foundation (Nos. S2013010014418 and 2014A030308013), Guangdong Talent Program (No. 201101D0104904202), Guangdong Innovative Research Team Program (No. 2011D039), and the Scientific Research Foundation of Graduate School of South China Normal University (No. 2014ssxm01).

[1]S. K. Cho, Y. J. Zhao, and C. J. Kim, Lab Chip **7**(4), 490–498 (2007).
[2]W. C. Nelson, I. Peng, G. A. Lee, J. A. Loo, R. L. Garrell, and C. J. Kim, Anal. Chem. **82**(23), 9932–9937 (2010).
[3]C. Peng, Z. N. Zhang, C. J. Kim, and Y. S. Ju, Lab Chip **14**(6), 1117–1122 (2014).
[4]C. S. Kim, ASME Trans. J. Fluids Eng. **129**(9), 1140–1146 (2007).
[5]J. Hong, Y. K. Kim, K. H. Kang, J. Kim, and S. J. Lee, Sens. Actuator, B Chem. **190**, 48–54 (2014).
[6]J. Hong, Y. K. Kim, K. H. Kang, J. Kim, and S. J. Lee, Sens. Actuator, B Chem. **196**, 292–297 (2014).
[7]A. G. Banpurkar, M. H. G. Duits, D. van den Ende, and F. Mugele, Langmuir **25**(2), 1245–1252 (2009).
[8]C. L. Hao, Y. H. Liu, X. M. Chen, Y. C. He, Q. S. Li, K. Y. Li, and Z. K. Wang, Sci. Rep. **4**, 6846 (2014).
[9]M. Im, K. Choi, D. H. Kim, J. H. Lee, J. B. Yoon, and Y. K. Choi, J. Adhes. Sci. Technol. **26**(12–17), 2079–2086 (2012).
[10]U. Levy and R. Shamai, Microfluid. Nanofluid. **4**, 97–105 (2008).
[11]R. Seemann, M. Brinkmann, E. J. kramer, F. F. Lange, and R. Lipowsky, Proc. Natl. Acad. Sci. U.S.A. **102**(6), 1848–1852 (2005).
[12]W. Y. Lu, T. Kim, A. J. Han, X. Chen, and Y. Qiao, J. Chem. Phys. **134**(20), 204706 (2011).
[13]N. Kumari and S. V. Garimella, Langmuir **27**(17), 10342–10346 (2011).
[14]M. Bienia, F. Mugele, C. Quilliet, and P. Ballet, Physica A **339**(1–2), 72–79 (2004).
[15]E. Seyrat and R. A. Hayes, J. Appl. Phys. **90**(3), 1383–1386 (2001).
[16]O. S. Kwon, M. Kim, T. Kim, C. Lee, S. Han, J. Y. Kim, C. H. Jung, J. H. Choi, and K. Shin, J. Nanosci. Nanotechnol. **11**(8), 7132–7136 (2011).
[17]J. C. Baret, M. M. J. Decre, and F. Mugele, Langmuir **23**(9), 5173–5179 (2007).
[18]H. Moon, S. K. Cho, R. L. Garrell, and C. J. Kim, J. Appl. Phys. **92**(7), 4080–4087 (2002).
[19]H. W. Lu, F. Bottausci, J. D. Fowler, A. L. Bertozzi, C. Meinhart, and C. J. Kim, Lab Chip **8**(3), 456–461 (2008).
[20]F. Mugele, Soft Matter **5**(18), 3377–3384 (2009).
[21]P. Sen and C. J. Kim, Langmuir **25**(8), 4302–4305 (2009).
[22]D. Mampallil, D. van den Ende, and F. Mugele, Appl. Phys. Lett. **99**(15), 154102 (2011).
[23]F. Mugele, A. Staicu, R. Bakker, and D. van den Ende, Lab Chip **11**(12), 2011–2016 (2011).
[24]P. Garcia-Sanchez and F. Mugele, in *Electrokinetics and Electrohydrodynamics in Microsystems*, edited by A. Ramos (Springer-Verlag Wien, Vienna, 2011), Vol. 530, pp. 85–125.
[25]J. C. Baret and F. Mugele, Phys. Rev. Lett. **96**(1), 016106 (2006).
[26]F. Mugele and J. Buehrle, J. Phys.-Condens. Matter **19**(37), 375112 (2007).
[27]D. T. Mannetje, F. Mugele, and D. van den Ende, Langmuir **29**(48), 15116–15121 (2013).
[28]S. R. Annapragada, S. Dash, S. V. Garimella, and J. Y. Murthy, Langmuir **27**(13), 8198–8204 (2011).
[29]N. Kumari, V. Bahadur, and S. V. Garimella, J. Micromech. Microeng. **18**(10), 085018 (2008).
[30]S. Dash, N. Kumari, and S. V. Garimella, J. Micromech. Microeng. **22**(7), 075004 (2012).
[31]F. Malloggi, D. van den Ende, and F. Mugele, Langmuir **24**(20), 11847–11850 (2008).
[32]F. Mugele, M. Duits, and D. van den Ende, Adv. Colloid Interface Sci. **161**(1–2), 115–123 (2010).
[33]F. Malloggi, H. Gu, A. G. Banpurkar, S. A. Vanapalli, and F. Mugele, Eur. Phys. J. E **26**(1–2), 91–96 (2008).
[34]W. C. Nelson and C. J. Kim, J. Adhes. Sci. Technol. **26**(12–17), 1747–1771 (2012).
[35]R. A. Hayes and B. J. Feenstra, Nature **425**, 383–385 (2003).
[36]L. L. Shui, R. A. Hayes, M. L. Jin, X. Zhang, P. F. Bai, A. van den Berg, and G. F. Zhou, Lab Chip **14**(14), 2374–2384 (2014).
[37]D. Y. Kim and A. J. Steckl, Langmuir **26**(12), 9474–9483 (2010).
[38]B. Sun, K. Zhou, Y. Lao, J. Heikenfeld, and W. Cheng, Appl. Phys. Lett. **91**(1), 011106 (2007).
[39]K. Zhou, J. Heikenfeld, K. A. Dean, E. M. Howard, and M. R. Johnson, J. Micromech. Microeng. **19**(6), 065029 (2009).
[40]J. Heikenfeld, 20th Annual Meeting of the IEEE Lasers and Electro–Optics Society, LEOS 2007 (2007), pp. 206–207.
[41]H. B. Eral, D. M. Augustine, M. H. G. Duits, and F. Mugele, Soft Matter **7**(10), 4954–4958 (2011).
[42]G. Beni and S. Hackwood, Appl. Phys. Lett. **38**(4), 207–209 (1981).
[43]G. Beni and M. A. Tenan, J. Appl. Phys. **52**(10), 6011–6015 (1981).
[44]J. Heikenfeld, K. Zhou, E. Kreit, B. Raj, S. Yang, B. Sun, A. Milarcik, L. Clapp, and R. Schwartz, Nat. Photonics **3**(5), 292–296 (2009).
[45]D. Klarman, D. Andelman, and M. Urbakh, Langmuir **27**(10), 6031–6041 (2011).
[46]H. You and A. J. Steckl, J. Soc. Inf. Disp. **21**, 192–197 (2013).
[47]J. Feenstra, in *Handbook of Visual Display Technology*, edited by J. Chen, W. Cranton, and M. Fihn (Springer, Berlin Heidelberg, 2012), pp. 1731–1745.
[48]A. Giraldo, R. Massard, J. Mans, E. Derckx, J. Aubert, and J. Mennen, SID Symp. Dig. Tech. Pap. **42**, 114–117 (2011).
[49]W. Y. Cheng, K. L. Lo, Y. P. Chang, C. W. Wang, P. J. Su, H. H. Lee, D. W. Lee, K. C. Lee, C. C. Hsiao, J. W. Shiu, S. Y. Fuh, Y. C. Liao, J. C. Yang, and C. H. Hsieh, SID Symp. Dig. Tech. Pap. **39**, 526–529 (2008).

[50]Z. Yi, L. Shui, L. Wang, M. Jin, R. A. Hayes, and G. Zhou, Displays **37**, 86–93 (2015).
[51]Y. S. Nanayakkara, H. Moon, T. Payagala, A. B. Wijeratne, J. A. Crank, P. S. Sharma, and D. W. Armstrong, Anal. Chem. **80**(20), 7690–7698 (2008).
[52]B. Koo and C. J. Kim, J. Micromech. Microeng. **23**(6), 067002 (2013).
[53]S. Berry, J. Kedzierski, and B. Abedian, Langmuir **23**(24), 12429–12435 (2007).
[54]X. Chen, T. He, H. Jiang, B. Wei, G. Chen, X. Fang, M. Jin, R. A. Hayes, G. Zhou, and L. Shui, Displays **37**, 79–85 (2015).
[55]J. C. Heikenfeld, N. R. Smith, B. Sun, K. Zhou, L. Hou, Y. Lao, and B. Raj, Proc. of SPIE **6887**, 688705 (2008).
[56]H. You and A. J. Steckl, Appl. Phys. Lett. **97**, 023514 (2010).
[57]R. Massard, J. Mans, A. Adityaputra, R. Leguijt, C. Staats, and A. Giraldo, J. Inf. Disp. **14**, 1–6 (2013).
[58]Y. Chiang and Y. Chao, Mater. Sci. Eng. B **177**, 1672–1677 (2012).
[59]S. Chevalliot, J. Heikenfeld, L. Clapp, and S. Viner, J. Disp. Technol. **7**(12), 649–656 (2011).
[60]Y. F. Chiang and Y. C. Chao, Mater. Sci. Appl. **05**, 485–490 (2014).
[61]F. Mugele and S. Herminghaus, Appl. Phys. Lett. **81**, 2303 (2002).
[62]J. Heikenfeld, B. Sun, K. Zhou, Y. Lao, and M. K. Kilaru, *Recent Advances in Electrowetting Display Fabrication, Device Architectures, and Performance* (Society Information Display Taipei Chapter, Taipei, 2007).
[63]L. Chen and E. Bonaccurso, Adv. Colloid Interfac. **210**, 2–12 (2014).
[64]Z. Yoshimitsu, A. Nakajima, T. Watanabe, and K. Hashimoto, Langmuir **18**, 5818–5822 (2002).
[65]M. Brinkmann and R. Lipowsky, J. Appl. Phys. **92**, 4296–4306 (2002).
[66]A. Klingner, S. Herminghaus, and F. Mugele, Appl. Phys. Lett. **82**(23), 4187–4189 (2003).
[67]B. Sun and J. Heikenfeld, J. Micromech. Microeng. **18**(2), 025027 (2008).
[68]T. Roques-Carmes, R. A. Hayes, B. J. Feenstra, and L. J. M. Schlangen, J. Appl. Phys. **95**(8), 4389–4396 (2004).
[69]F. Mugele and J.-C. Baret, J. Phys.: Condens. Matter **17**, R705 (2005).